Iranian Journal of Chemistry and Chemical Engineering (IJCCE)

Cellulose-supported Ni/Al Layered Double Hydroxide (LDH) as Unique Adsorbents for Malachite Green Dye Removal in Aqueous Solutions

Alfan Wijaya; Zaqiya Artha Zahara; Patimah Mega Syah Bahar Nur Siregar; Nur Ahmad; Amri Amri

Research Centre of Inorganic Materials and Complexes, Graduate School, Universitas Sriwijaya, South Sumatera, INDONESIA

Neza Rahayu Palapa

Department of Chemistry, Faculty of Mathematics and Natural Sciences, Universitas Sriwijaya, South Sumatera, INDONESIA

Risfidian Mohadi, Aldes Lesbani*+

Research Centre of Inorganic Materials and Complexes, Universitas Sriwijaya, South Sumatera, INDONESIA
Master Program of Material Science, Graduate School, South Sumatera, INDONESIA

**Corresponding author email: aldeslesbani@pps.unsri.ac.id*

ABSTRACT: *Ni/Al-cellulose composites were successfully synthesized using the co-precipitation method. X-ray Diffraction (XRD), Fourier Transform infrared spectroscopy (FT-IR), Scanning Electron Microscope (SEM), and Brunauer-Emmett-Teller (BET) were used to characterize the structure of materials. Ni/Al-cellulose was applied to the malachite green dye (MG) adsorption process to study adsorption and reusability performance. The surface area of Ni/Al material after composting with cellulose increased, from 3.288 to 5.096 m^2/g. The optimum pH for MG was pH 7 and pH PZC > pH optimum. The equilibrium contact time is 150 minutes. The MG adsorption process in this experiment follows the Langmuir isotherm and pseudo second order kinetic models. The adsorption process occurs through physisorption and chemisorption (physicochemical process) based on kinetic data, isotherm data, ΔG value, pH optimum ≠ pH PZC, and FT-IR results of adsorbent after MG adsorption. Ni/Al-cellulose has adsorption capacity and percent removal of 107.527 mg/g (71%). Reusability studies show that Ni/Al-cellulose is more effective for reusable in the adsorption process of MG until the sixth cycle, with an adsorption capacity of 54%. Thus, the synthesized NiAl/cellulose composites could be potentially used as an efficient adsorbent for MG adsorption in wastewater.*

KEYWORDS: *Cellulose, Modified LDH, Co-precipitation method, Adsorption, Malachite green, Reusability performance*

INTRODUCTION

The rapid development of the textile industry in Indonesia not only provides benefits but also harms the environment [1]. This is because in its production the textile industry always produces waste, namely dye waste [2]. The waste produced from the dye is an organic substance that is complicated to degrade [3], resistant [4], and toxic [5]. This dye waste when discharged into the waters will cause environmental pollution. One of the dyes found in the textile industry is malachite green (MG) [6]. MG is a cationic dye with a dark green color that is frequently used in the textile industry and the form of a crystalline solid. The chemical structure, physical, and chemical characteristics of the MG dye are shown in Fig. 1 and Table 1.

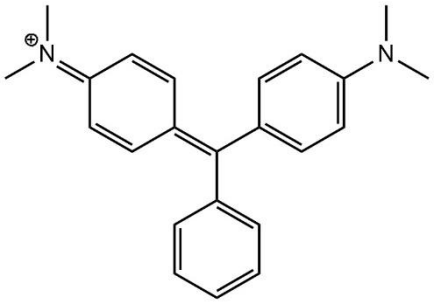

Fig. 1: Chemical structure of MG

Table 1. The physical and chemical characteristics of the MG [7]

Molecular weight	***364.91 g/mol***
Melting point	***164°C***
Complexity	***516***
Max absorption	***616.9 nm***
Color/form	***Green crystals with metallic luster***
Solubility	***Soluble in water, ethanol, methanol, amyl alcohol***

MG is often used in the production of ceramics and textiles, biocides in the aquaculture industry and to treat fungal and bacterial infections of fish skin because of its very high disinfection efficiency. Additionally, MG is utilized as a food additive, medicinal disinfectant, food coloring agent, and dye in the paper, silk, wool, hemp, cotton, leather, and acrylic industries so that it affects the immune and reproductive system, genotoxic and carcinogenic [3]; [8-9]. Several methods can be used to solve the dye waste problem, including coagulation [10], electrochemical degradation [11], photodegradation [12], and adsorption methods [13]. An alternative and effective method of dye removal is using adsorption. The adsorption method is the most profitable because the process is simple, has high adsorption effectiveness and capacity, is selective, has low operational costs, and does not provide side effects in the form of toxic substances [14-16]. Various kinds of adsorbents can be used in the adsorption process, such as zeolite [17], clay [18], cellulose [19], and layered double hydroxide (LDH) [20]. Due to its vast variety, controlled layer spacing, and excellent adsorption capacity, LDH is one of the layered materials as a new and popular adsorption material in dye removal [21]. Zn-Fe LDH, which has an adsorption capacity of 71.74 mg/g, was found to be effective at removing MG from an aqueous solution, according to research by

Mammoud et al [22]. Cu/Al LDH, which has an adsorption capacity of 55.86 mg/g, can be utilized as an adsorbent in the process of removing MG, according to Palapa et al [23]. Since LDH's structure is easily broken, it cannot be reusable in the adsorption process, the use of LDH as an adsorbent directly in the process of eliminating dye waste in the water is still less effective. It can cause new problems because it results in the emergence of adsorbent waste that has been used, so it is necessary to modify the LDH using a supporting material to obtain a reusable adsorbent (reusability). Research conducted by Brahma et al [24] reported that modified CoAl-LDH with Coconut Husk Ash Fabricated shows 3 cycles of reusability performances on MG dye removal with an adsorption percentage of 60.3% in the third cycle. This proves that LDH modification with carbon-based materials will improve adsorption ability and reusability performance.

This research aims to improve the ability of modified materials on the adsorption of organic pollutants, namely MG dye. In this study, a modification process was carried out on LDH using a support material in the form of cellulose to obtain a material that can be used repeatedly in the adsorption process. This modified material will be a unique adsorbent with high reusability and adsorption performance and it will be a novelty and excellence in this research. The materials were synthesized using the coprecipitation method. The coprecipitation method has advantages including simple, quick preparation, and the temperature used is relatively low so it is energy efficient. The synthesized materials were characterized using X-ray Diffraction (XRD), Fourier Transform infrared spectroscopy (FT-IR), Scanning Electron Microscope (SEM), and Brunauer-Emmett-Teller (BET) to verify the success of the material preparation. Afterward, the synthesized materials were applied as an adsorbent during the MG dye adsorption process. Variations in time, concentration, and temperature were used throughout the adsorption process, and the adsorbent's ability to be reused for eight cycles was also studied.

EXPERIMENTAL SECTION

Chemical and Instrumentation

In this study, the chemicals used were $Ni(NO_3)_2.6H_2O$ by Merck, $Al(NO_3)_3.9H_2O$ by Sigma Aldrich, cellulose by Merck, and distilled water by Bratachem Inc., HCl by Merck, NaOH by Sigma Aldrich, Na_2CO_3 by EMSURE® ACS, and MG dye. The XRD analysis of the Rigaku Miniflex-6000, the FTIR analysis of the Shimadzu Prestige-21, and the SEM analysis of the SU 8000 series were used to characterize the materials. and the Determination of absorbance from the filtrate used UV-Vis spectrophotometer Biobase BK-UV 1800 PC.

Synthesis Ni/Al

The coprecipitation method was used to synthesize LDH (Ni/Al). A total of 50 mL of 2 M NaOH was mixed with 100 mL of 0.3 M Na_2CO_3 solution. The mixture was dripped with 100 mL of 0.25 M $Al(NO_3)_3.9H_2O$ solution, 100 mL of 0.75 $Ni(NO_3)_2.6H_2O$ solution, and adjust the pH of the solution was to 10 using NaOH 2 M. At 80°C, the mixture was stirred for 17 hours. The precipitate was washed, dried in a 100°C oven for 24 hours, and then filtered. XRD, FT-IR, SEM, and BET were used to characterize the synthesized materials.

Preparation of Ni/Al-cellulose

30 mL of 0.25 M $Ni(NO_3)_2.6H_2O$ and 30 mL of 0.75 M $Al(NO_3).9H_2O$ were put into a beaker glass. The mixture was adjusted to pH up to 10 using 2 M NaOH, and then 3 g of cellulose was added after the mixture had been agitated for an hour. At 80°C, the mixture was stirred for 72 hours. The solids were filtered, cleaned, dried, and subjected to XRD, FT-IR, SEM, and BET characterization.

pH point zero charge (PZC) Study

In order to do a pH PZC, 20 mL of 0.1 M NaCl solution that had been adjusted to pH 2, 3, 4, 5, 6, 7, 8, 9, and 11 with 0.1 M NaOH and HCl solutions was added with 0.02 g of adsorbent. The liquid is filtered and the final pH is determined using a pH meter after 24 hours of stirring. The pH PZC of each drug was determined by calculating the connection between the initial pH and the final pH.

Adsorption Experiment of MG

Effect of Variation pH

Variations of pH 2-10 were utilized to examine the effects of the solution's pH by adding NaOH 0.01 M and HCl 0.01 M. 0.015 grams of Ni/Al, cellulose, and Ni/Al-cellulose adsorbents were combined with 50 mg/L of malachite green, and the mixture was agitated for two hours. The filtrate's absorbance was then determined using a UV-Vis spectrophotometer at 617 nm. The adsorption capacity (qe) was determined following Equation (1).

$$qe = \frac{(C_0 - C_t) \times V}{w} \quad (1)$$

where C_0 is the initial concentration of MG (mg/L), C_t is the concentration of MG at time equilibrium (mg/L), V is the volume of MG (L), and w is the mass of adsorbents (g).

Kinetic Study

15 mL of MG solution was put in 13 beaker glasses and added with 0.015 grams of adsorbents (Ni/Al, cellulose, and Ni/Al-cellulose). The solution was stirred with variations of time (5, 10, 20, 30, 40, 50, 60, 70, 90, 120, 150, 180, and 200 minutes), and with the use of a UV-Vis spectrophotometer, the absorbance value of the filtrate is measured at each time.

Effect of Concentration and Temperature

The effect of malachite green concentration on the adsorbent was studied by varying the concentration (30, 35, 40, 45, 50, 70, 90, 110, 130 mg/L). 15 mL of malachite green solution was added with 0.015 grams of adsorbent (Ni/Al, cellulose, Ni/Al-cellulose) and stirred for 150 minutes at temperatures (30, 40, 50, 60, 70°C). After the stirring was completed, with the use of a UV-Vis spectrophotometer, the filtrate's absorbance value was measured.

Reusability Performance

The reusability process was carried out with 20 mL of malachite green at 100 mg/L by adding 0.02 gram of adsorbent (Ni/Al, cellulose, Ni/Al-cellulose) and the mixture was stirred for 150 minutes. After the stirring process was completed, with the use of a UV-Vis spectrophotometer, the filtrate's absorbance value was measured. 20 mL of distilled water was added after the remaining adsorbent had dried, and then desorbed with ultrasonic equipment. The remaining desorption adsorbent was dried for use in the next adsorption process up to eight times.

RESULTS AND DISCUSSION

Characterization of Adsorbent

XRD Analysis

The results of the XRD analysis of each adsorbent are shown in Fig. 2. Fig. 2(a) shows the diffractogram pattern of Ni/Al, the peaks appearing at an angle of 2θ = 11.57°(003), 22.91°(006), 35.04°(012), 39.73°(015), and 61.9°(110). Normah et al., [25] said that the diffraction peaks of Ni/Al are at angles of 11.63°(003), 23°(006), and 61.59°(110), according to JCPDS data No.40-0216. The diffraction peaks of cellulose appeared at angles of 15.19°(110) and 22.67°(006), as shown in Fig. 2(b). Research conducted by Ishak et al., [26] confirmed that the diffraction angles for cellulose were 16°, 22°, and 35° following JCPDS data No. 00-056-1718. The diffractogram of Ni/Al-cellulose can be seen in Fig. 2(c). In the Fig. 2(c) shows the diffraction angles at 11.65°(003), 22.85°(006), 29.397°(009), 35.10°(012), and 61.1°(110). According to research by Allou et al [27], the diffraction angle was 11.40° with the planes (003), (006), (009), (110), and (113).

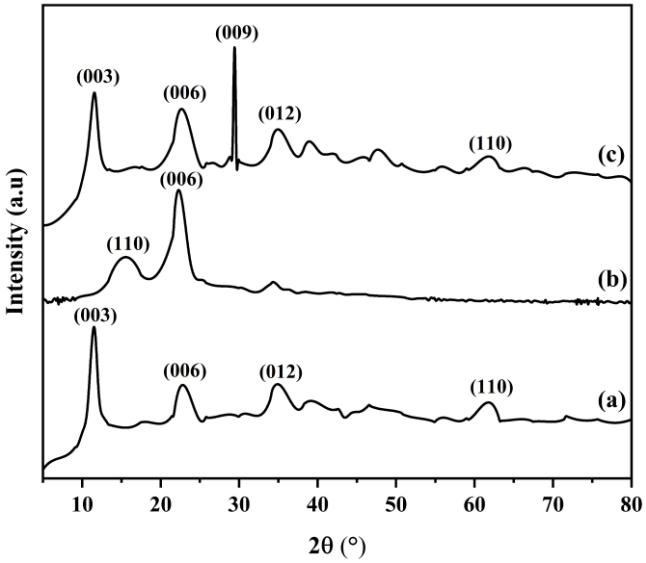

Fig. 2: XRD diffractogram of Ni/Al (a), cellulose (b), Ni/Al-cellulose (c)

FT-IR Analysis

The results of the FTIR analysis of the Ni/Al, cellulose, and Ni/Al-cellulose adsorbents are shown in Fig. 3. Fig. 3(a) is the result of FTIR analysis of Ni/Al which shows a wide vibration at a wavenumber of 3502 cm^{-1} which indicates the presence of O-H groups in water molecules. The O-H bending vibration has the wavenumber 1635 cm^{-1}. The wavenumber in the 1381 region indicates the NO_3^- anion group. M-O (metal groups) are present, as shown by the wavenumber 740-347 cm^{-1}. Research conducted by Normah et al., 2021 [25] shows that the spectrum of Ni/Al appears at wavenumbers 3464, 1635, 1381, and 748 cm^{-1}.

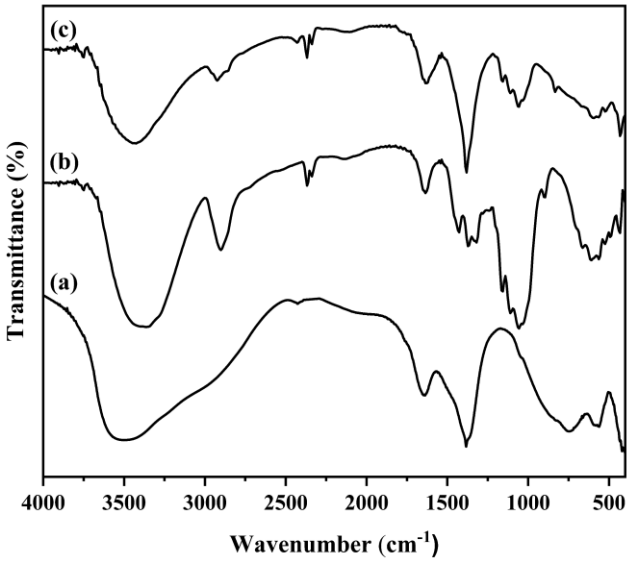

Fig. 3: FT-IR spectrum of Ni/Al (a), cellulose (b), Ni/Al-cellulose (c)

The cellulose FT-IR spectra was presented in Fig. 3(b). A broadened vibration at wave number 3363 cm^{-1} indicates the presence of groups O-H [28]. C-H group is present, as indicated by the wavenumber of 2900 cm^{-1}. The wavenumber of 1057 cm^{-1} indicates the presence of a C-O group. The results of research conducted by Jia et al [29] show the results of the FT-IR spectrum for cellulose at a wavenumber of 3390 cm^{-1} for the O-H group. The C-H group is found at the wavenumber 2905 cm^{-1}. The wavenumber of 1059 cm^{-1} is found in the C-O group.

The Ni/Al-cellulose spectrum in Fig. 3(c) shows that The presence of O-H groups can be seen in the FTIR spectra at a wavenumber of 3425 cm^{-1}. O-H bending vibrations are shown by the wavenumber at 1635 cm^{-1}. The wavenumber of 1381 cm^{-1} indicates the presence of the NO_3^- anion group from LDH. The C-H group is found at the wavenumber 2900 cm^{-1}. The C-O group was found at a wavenumber of 1056 cm^{-1} which was derived from cellulose. The M-O group can be seen at the wavenumber 748-563 cm^{-1}.

BET Analysis

The results of the BET analysis can be seen in Fig. 4 and Table 2. Based on the data in Fig. 4, the BET isotherm type follows type IV with the presence of hysteresis phenomena that indicate the presence of non-uniform material pores and according to Table 1, the surface area of the Ni/Al material increased after being composted with cellulose, from 3.288 to 5.096 m^2/g. This proves that the process of modifying Ni/Al material with cellulose forming Ni/Al-cellulose can increase the surface area of the material. The material in this study is included in the mesoporous material. Mesoporous materilas have pores that range in size from 2 to 50 nm, according to IUPAC. These mesoporous materials have a unique structure that provides a large surface area and high pore volume, thus making them attractive for various applications, such as adsorption.

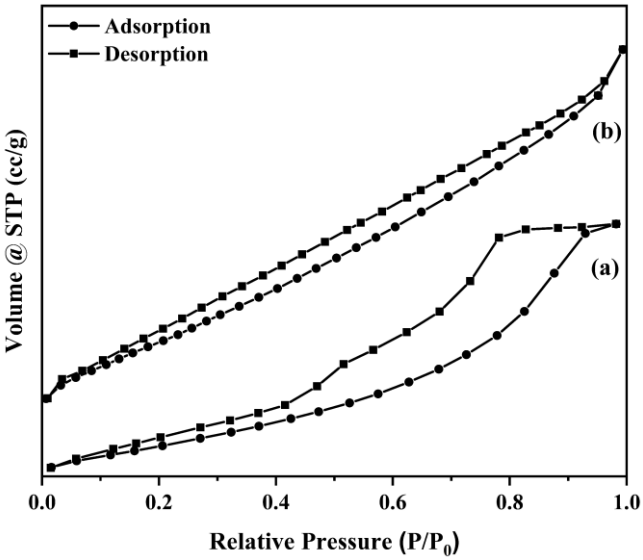

Fig. 4: N_2 adsorption-desorption properties of the Ni/Al (a) and Ni/Al-cellulose (b)

Table 2: BET surface area, pore size, and pore volume of Ni/Al and Ni/Al-cellulose

Adsorbents	*Surface Area (m^2/g)*	*Pore Size (nm)*	*Pore Volume (cm^2/g)*
Ni/Al	*3.288*	*19.102*	*0.007*
Ni/Al-cellulose	*5.096*	*16.833*	*0.004*

SEM Analysis

SEM analysis aims to determine a material's morphology, topography, shape, and size. Fig. 5 shows the results of the analysis of each adsorbent using SEM. Fig. 5(a) shows the morphology of Ni/Al with a magnification of 10 μm, having a rough surface with a large flat plate shape but not larger than Ni/Al-cellulose. Fig. 5(b) shows the results of the SEM analysis, confirming that the morphology of the Ni/Al-cellulose composite with a magnification of 50 μm has an irregular shape and the aggregate is larger than that of Ni/Al.

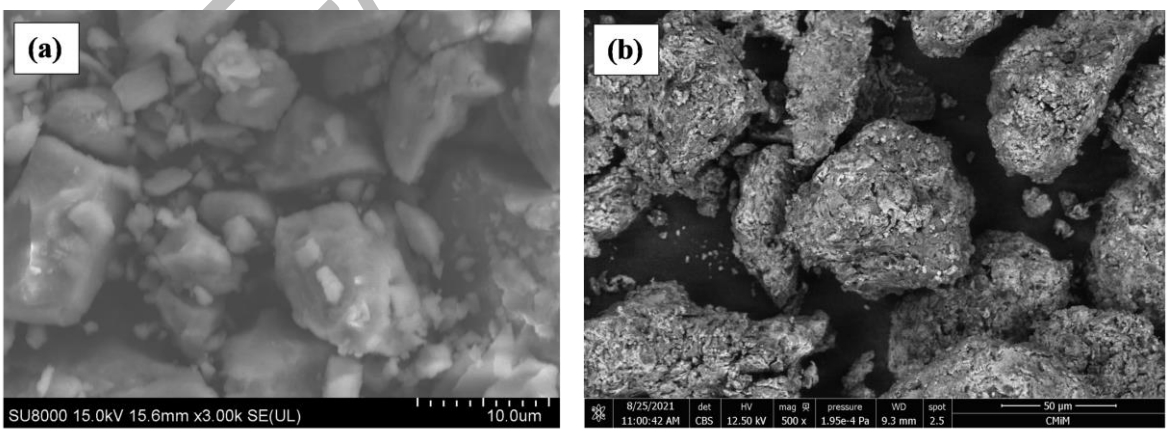

Fig. 5: SEM analysis of Ni/Al (a) and Ni/Al-cellulose (b)

Adsorption Study of MG

Effect of Variation pH

Fig. 6 shows how each adsorbent's pH has an influence. The MG adsorption process uses Ni/Al, cellulose, and Ni/Al-cellulose adsorbents with an optimum pH of 7. At acidic pH conditions, many H^+ ions will cause a

repulsive force between the adsorbent and the MG dye which is categorized as a cationic dye, so it can cause the adsorption process to be not optimal. Deprotonation and electrostatic or tensile force between the negatively charged surface and the positively charged MG occurs under alkaline pH conditions. This is because at alkaline pH there is an excess of OH^- ions and a change in the structure of the MG dye occurs [30]. therefore, the MG adsorption process is more effectively carried out at pH 7 which at that pH is the normal pH of MG.

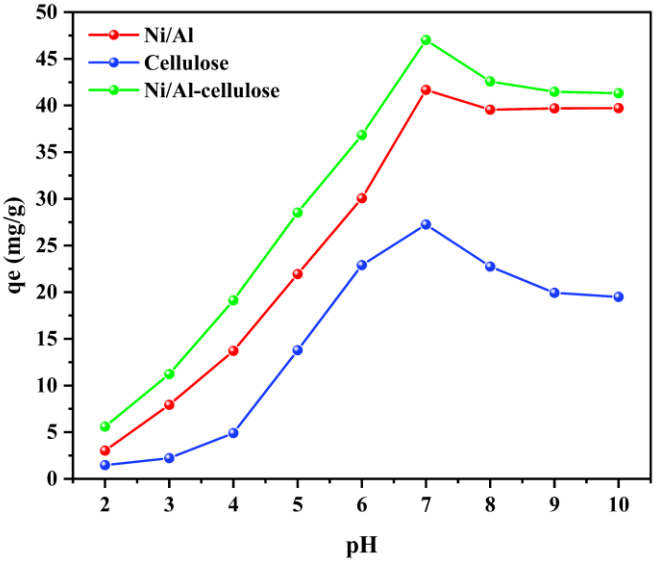

Fig. 6: Effect of variation pH MG on Ni/Al, cellulose, and Ni/Al-cellulose (Experimental conditions: pH= 2-10; time= 120 minutes; adsorbent mass= 0.015 g; dye solution volume: 15 mL; concentration= 50 mg/L)

To identify the adsorption mechanism that occurred, pH PZC was performed. The pH PZC of Ni/Al, cellulose, and Ni/Al-cellulose (in Fig. 7) were pH 9.26, 9.05, and 9.47. In theory, the adsorbent surface will be positively charged if the adsorbent's pH value is below pH PZC, and negatively charged if the adsorbent's pH value is above pH PZC. Cationic dyes that are positively charged are more suitable above pH PZC. However, this research resulted in an optimum pH of MG adsorption of 7 (below pH PZC), so it is assumed that other interactions occur. According to Ahmad et al., [13] physisorption and chemisorption occur at pH optimum ≠ pH PZC.

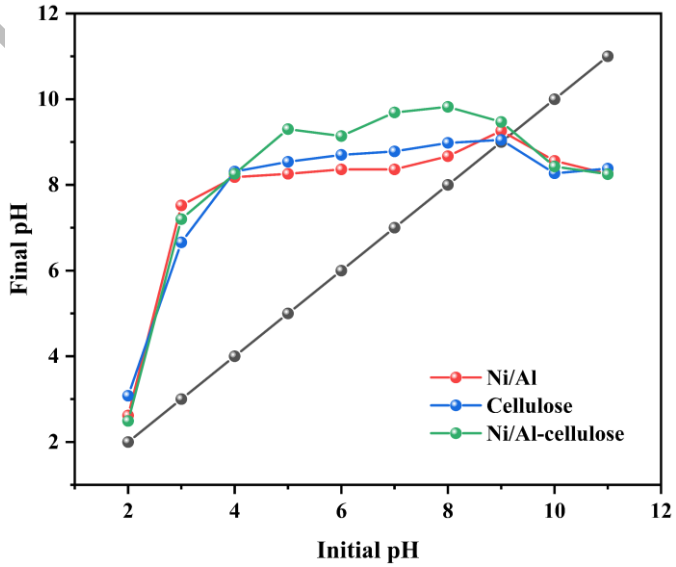

Fig. 7: pH point zero charges (PZC) of Ni/Al, cellulose, and Ni/Al-cellulose

The hydrogen interaction and π-π interaction are assumed to occur when the MG adsorption process with adsorbents. The FTIR spectrum after adsorption can prove the mechanism of adsorption, as shown in Fig. 8. The sharper peak intensities at 3441 and 1620 cm^{-1} indicate the typical absorption of O-H bonds from the adsorbent with MG, in addition, there is a shift in wavenumbers indicating chemical interactions that occur in the adsorption process. Fig. 9 shows the schematic illustration of the mechanism of MG.

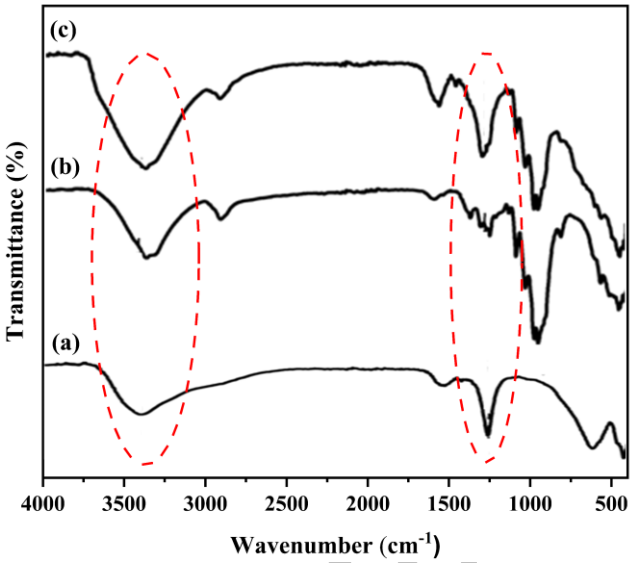

Fig. 8: FTIR of Ni/Al (a), cellulose (b), and Ni/Al-cellulose (c) after MG adsorption

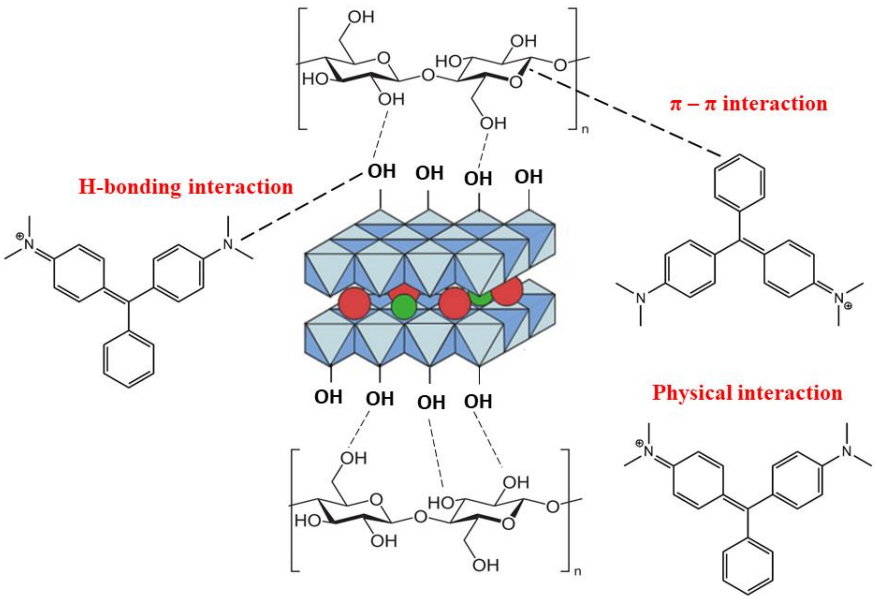

Fig. 9: Schematic illustration of the adsorption mechanism of MG

Kinetic Study

Fig. 10 shows the results of the effect of the contact time between the adsorbate and the adsorbent. Based on Fig. 10, the amount of MG on Ni/Al, cellulose, and Ni/Al-cellulose increased with the increasing contact time until equilibrium was reached. In the early minutes, the adsorption of MG occurs rapidly, then it takes longer to reach equilibrium at 150 minutes. The presence of an insignificant increase in the amount of MG adsorbed on

Ni/Al, cellulose, and Ni/Al-cellulose is an indication that equilibrium has been reached. In this study, three adsorption kinetic parameters were fitted to the experimental data; pseudo first order, pseudo second order, and intraparticle diffusion. The equation for pseudo first order, pseudo second order, and intraparticle diffusion are defined in Equations (2), (3), and (4), respectively [13].

$$\log (qe - qt) = \log qe - \left(\frac{k_1}{2{,}303}\right)t \qquad (2)$$

$$\frac{t}{qt} = \frac{1}{k_2 q_e^{\,2}} + \frac{1}{q_e}\,t \qquad (3)$$

$$qt = k_{diff}\, t^{0.5} \qquad (4)$$

where qe is the adsorption capacity at equilibrium (mg/g), qt is the adsorption capacity at time t (mg/g), t is contact time (min), k1 is equilibrium rate constant for the pseudo first order model (min^{-1}), k_2 is equilibrium rate constant for the pseudo second order model (g/mg.min), and k_{diff} is the intraparticle diffusion constant ($mg/g.min^{-1/2}$).

In Table 3, it is shown that the adsorption kinetics of Ni/Al, cellulose, and Ni/Al-cellulose generally follow the pseudo second order kinetic model rather than the pseudo first order, and intraparticle diffusion with the linear regression value (R^2), which is closer to 1, and the similarity between the experimental qe value and the calculated qe [17]. According to this concept, chemisorption is how adsorption takes place, and the adsorption rate is dependent on adsorption capacity rather than adsorbate concentration.

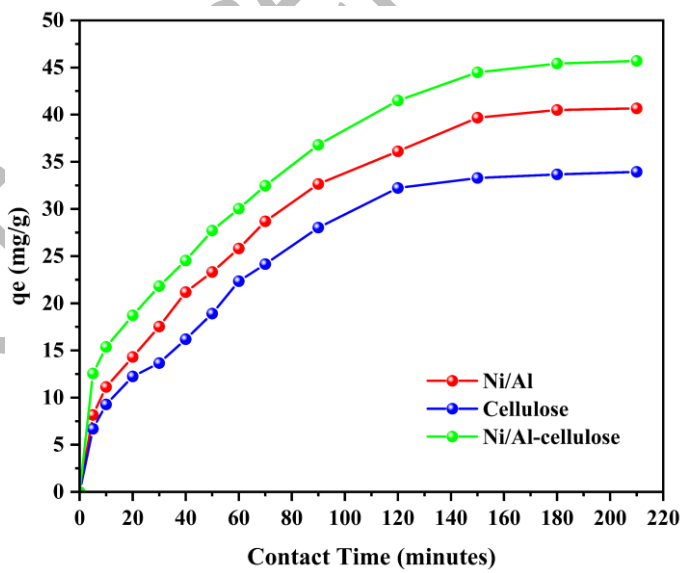

Fig. 10: Effect of contact time adsorption of MG on the adsorbent Ni/Al (a), cellulose (b), and Ni/Al-cellulose (c) (Experimental conditions: pH= 7; time= 5-210 minutes; adsorbent mass= 0.015 g; dye solution volume: 15 mL; concentration= 50 mg/L)

Table 3. Kinetic parameters of Ni/Al, cellulose, and Ni/Al-cellulose

Adsorbents	$qe_{experiment}$ *(mg/g)*	*Pseudo first order*			*Pseudo second order*			*Intraparticle diffusion*	
		qe_{Calc} *(mg/g)*	R^2	*k1*	qe_{Calc} *(mg/g)*	R^2	*k2*	k_{diff}	R^2
Ni/Al	*40.669*	*53.186*	*0.921*	*0.026*	*50*	*0.980*	*0.0004*	*2.980*	*0.976*
Cellulose	*33.938*	*36.551*	*0.940*	*0.021*	*42.553*	*0.971*	*0.0004*	*2.540*	*0.970*
Ni/Al-cellulose	*45.706*	*52.905*	*0.942*	*0.024*	*53.476*	*0.980*	*0.0005*	*3.176*	*0.975*

Effect of Concentration and Temperature (Isotherm and Thermodynamic Studies)

Fig. 11 shows that as concentration and temperature were increased for the Ni/Al, cellulose, and Ni/Al-cellulose adsorbents, the amount of adsorbed MG also increased significantly. The adsorption isotherm can be used to study changes in the adsorbate concentration during the adsorption process. The Langmuir and Freundlich type adsorption isotherm is the most commonly used type [31]. Plotting the Langmuir and Freundlich adsorption isotherm equations into a straight-line equilibrium curve, where the equilibrium model depends on a linear regression value (R^2) close to 1, was done to identify the adsorption isotherm parameter [32]. The mechanism of adsorption in adsorbents towards adsorbates can be identified using this form of adsorption isotherm. Bonds between the molecules of the adsorbate and the adsorbent surface form through physisorption and chemisorption in solid-liquid phase adsorption, which typically follows the Langmuir and Freundlich types of adsorption isotherms [33-34]. In addition, the Temkin isotherm model was fitted to experimental data in this work. This model of adsorption isotherms applies only to the intermediate concentration range. The Temkin isotherm model ignores very high and low concentration values while considering the interaction between adsorbents and adsorbate [35]. The linear equation of Langmuir, Freundlich, and Temkin isotherm models are expressed by Equations (5), (6), and (7), respectively [34-35].

$$\frac{C_e}{q_e} = \frac{C_e}{Q_{max}} + \frac{1}{Q_{max} K_L} \quad (5)$$

$$\text{Log } q_e = \log K_F + 1/n \log C_e \quad (6)$$

$$qe = \frac{RT}{b_T} \ln Kt + \frac{RT}{b_T} \ln Ce \quad (7)$$

where Ce is the concentration of the dye solution at the equilibrium (mg/L), qe is the adsorption capacity at the equilibrium (mg/g), Q_{max} is the maximum adsorption capacity (mg/g), 1/n is the empirical parameter associated with surface heterogeneity, K_L is the adsorption constant of the Langmuir model (L/g), K_F is the adsorption constant of the Freundlich model (mg/g $(L/g)^{-1/n}$), where Kt is the equilibrium binding constant (L/g), b is the heat of adsorption (J/mol), R is the gas constant (8.314 J/K/ mol), and T is the temperature in Kelvin.

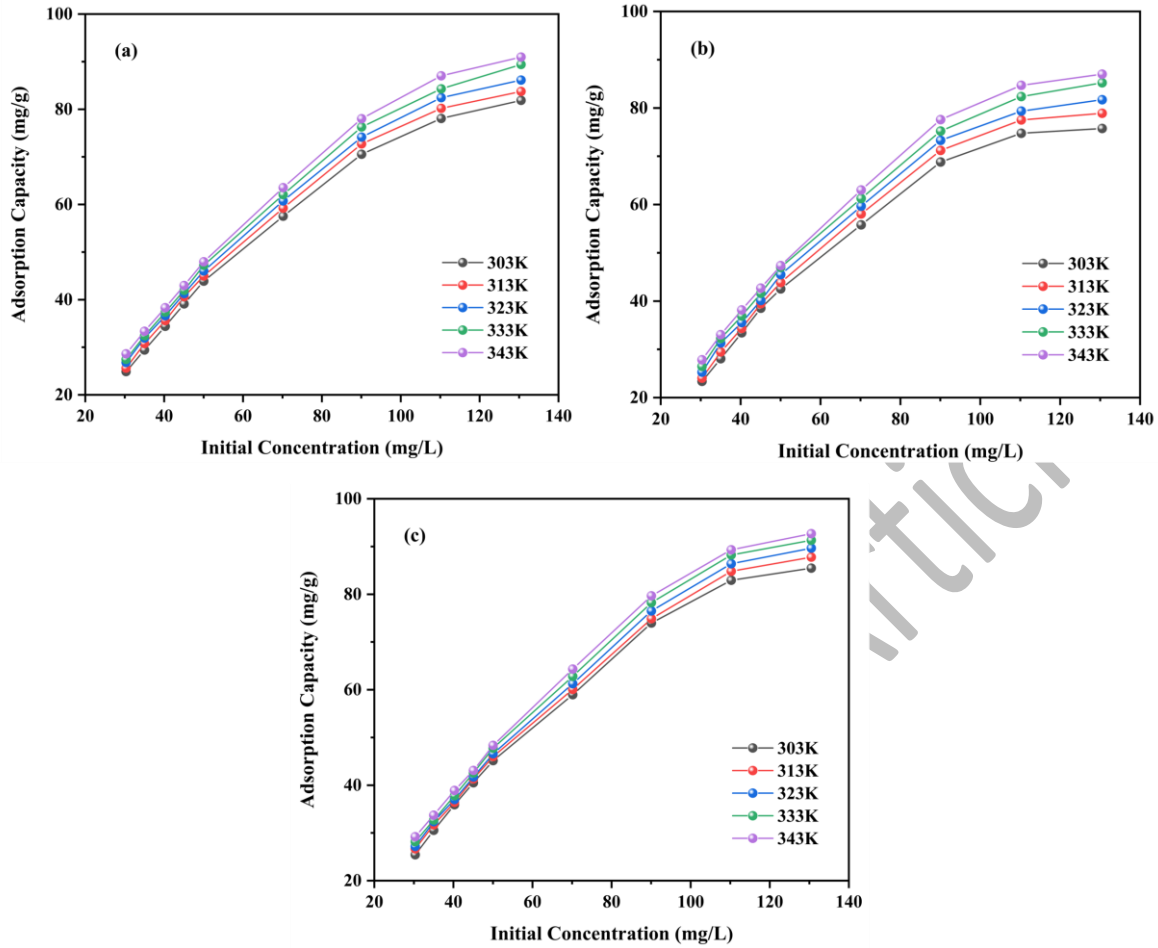

Fig. 11: Effect of concentration and temperature adsorption of MG onto Ni/Al (a), cellulose (b), and Ni/Al-cellulose (c) (Experimental conditions: pH= 7; time= 150 minutes; adsorbent mass= 0.015 g; dye solution volume: 15 mL; concentration= 30, 35, 40, 45, 50, 70, 90, 110, 130 mg/L; temperature= 303, 313, 323, 333, and 343K)

Table 4. Adsorption isotherms of MG dye on Ni/Al, cellulose, and Ni/Al-cellulose (Temperature= 343K)

Adsorbents	*Adsorption Isotherm*	*Constants*	
Ni/Al	*Langmuir*	Q_{max} *(mg/g)*	*104.167*
		kL (L/mg)	*0.106*
		R^2	*0.966*
	Freundlich	*n*	*2.101*
		kF (mg/g) (L/mg)$^{1/n}$	*14.949*
		R^2	*0.851*
	Temkin	K_T *(L/mg)*	*0.717*
		b_T *(J/mol)*	*24.612*
		R^2	*0.936*
Cellulose	*Langmuir*	Q_{max} *(mg/g)*	*100*
		kL (L/mg)	*0.070*
		R^2	*0.927*
	Freundlich	*n*	*2.049*
		kF (mg/g) (L/mg)$^{1/n}$	*12.832*
		R^2	*0.792*
	Temkin	K_T *(L/mg)*	*0.064*
		b_T *(J/mol)*	*46.073*
		R^2	*0.977*
Ni/Al-cellulose	*Langmuir*	Q_{max} *(mg/g)*	*107.527*
		kL (L/mg)	*0.102*
		R^2	*0.964*
	Freundlich	*n*	*2.162*
		kF (mg/g) (L/mg)$^{1/n}$	*17.314*
		R^2	*0.841*
	Temkin	K_T *(L/mg)*	*0.894*
		b_T *(J/mol)*	*24.988*
		R^2	*0.927*

The pattern of the MG adsorption isotherm by each adsorbent used can be identified using Table 4. According to Table 4, the adsorption isotherm of MG was best fitted by the Langmuir model rather than the Freundlich and Temkin models. The Langmuir model exhibited the highest R^2 values. This indicates that a homogenous adsorbent surface and a monolayer of adsorbed MG are formed. The Langmuir isotherm model is based on the formation of an adsorbate monolayer layer with a homogeneous adsorbent surface, and the Langmuir isotherm indicates a chemisorption adsorption process [9].

Based on the isotherm data, the concentration increase is inversely correlated to the adsorption capacity. With increased concentration, the ability of MG for adsorption increased. Additionally, Table 4 indicates that

Ni/Al-cellulose has a higher maximum adsorption capacity than Ni/Al and cellulose, with values of 107.527 mg/g, 104.167 mg/g, and 100 mg/g and percent removal of 71%, 69.8%, and 66.6%, respectively.

Table 5. Thermodynamic parameters onto Ni/Al, cellulose, and Ni/Al-cellulose

Adsorbents	*T (K)*	*Q_e (mg/g)*	*ΔH (kJ/mol)*	*ΔS (J/mol K)*	*ΔG (kJ/mol)*
Ni/Al	*303*	*81.750*	*7.124*	*0.028*	*-1.280*
	313	*83.750*			*-1.557*
	323	*86.375*			*-1.834*
	333	*89.125*			*-2.112*
	343	*91.063*			*-2.389*
Cellulose	*303*	*75.800*	*8.246*	*0.030*	*-0.812*
	313	*78.675*			*-1.111*
	323	*81.613*			*-1.410*
	333	*85.488*			*-1.709*
	343	*86.925*			*-2.008*
Ni/Al-cellulose	*303*	*85.738*	*5.129*	*0.022*	*-1.654*
	313	*88.050*			*-1.878*
	323	*89.425*			*-2.102*
	333	*90.988*			*-2.325*
	343	*92.613*			*-2.549*

The thermodynamic parameters of enthalpy data (ΔH), entropy value (ΔS), and Gibbs free energy (ΔG) [36] were evaluated using the information on the effect of temperature on the adsorption of MG using Ni/Al, cellulose, and Ni/Al-cellulose. The thermodynamic parameters were expressed by Equations (8) and (9).

$$\ln \frac{qe}{Ce} = \frac{\Delta S}{R} - \frac{\Delta H}{RT} \quad (8)$$

$$\Delta G = \Delta H - T\,\Delta S \quad (9)$$

where T is the temperature (in Kelvin), R is the gas constant (8.314 J/K/ mol), ΔH is the enthalpy (kJ/mol), ΔS is the entropy (J mol/K), and ΔG is Gibbs free energy (kJ/mol).

Thermodynamic parameter data for Ni/Al, cellulose, and Ni/Al-cellulose are shown in Table 5. Enthalpy's positive value in Table 4 shows that the adsorption process is endothermic. Chemical reactions, an increase in the reactivity of adsorbent surface sites, and the diffusion of adsorbate ion particles into the adsorbent's pores can all result in endothermic properties [37]. In addition, the enthalpy value for MG adsorption on all materials is lower than 40 kJ/mol indicating the adsorption process occurs in physisorption [38], while the ΔG value is in the range of 0 to -20 $kJ.mol^{-1}$ which indicates the presence of physical adsorption [39]. However, the isotherm data follows the Langmuir isotherm model where the adsorption process occurs chemisorption [9] and the pH test shows a difference in the optimum pH and pH PZC, proving that both physisorption and chemisorption happen (physicochemical process) [13]. Each adsorbent has a low entropy value (ΔS), which indicates that there is a small degree of irregularity in the adsorption process. Positive ΔS values indicate a more random organization of the adsorbate at the solid or solution interface, while negative values indicate the opposite fact [39]. To determine the

spontaneity of the reaction, the Gibbs free energy of a system indicates a change in the entropy of the entire system. Gibbs-free energy is negative, which means that the adsorption process occurs spontaneously [33]. Table 6 shows the adsorption capacity of MG with various adsorbents. It is proven from the table that the adsorbents used in this study have advantages over other adsorbents in terms of their adsorption ability.

Table 6. The adsorption capacity of MG with other adsorbents

Adsorbents	*Adsorption Capacity (mg/g)*	*References*
Rice Husks	***6.5***	[40]
Ficus cartia	***51.79***	[41]
Acid-activated carbon	***32.787***	[33]
Musa balbisiana Colla	***8.066***	[42]
Nutraceutical Industrial Pterocarpus Marsupiumspent	***45***	[43]
Lignin	***31.2***	[44]
Activated Carbon from Snail Shell	***1.754***	[45]
Charred Wheat Bran	***8.29***	[46]
natural red clay	***84.75***	[47]
Fly Ash	***2.23***	[48]
Mangan Oxide-assisted in Biochar	***79.365***	[49]
Mesoporous Pyrophanite- MnTiO3/TiO2 Nanoparticles	***11.764***	[50]
Ni/Al	***104.167***	***This Research***
Cellulose	***100***	***This Research***
Ni/Al-cellulose	***107.527***	***This Research***

Reusability Performance

Fig. 12 shows the results of the reusability of Ni/Al, cellulose, and Ni/Al-cellulose adsorbents. **Fig. 12** indicates that Ni/Al-cellulose has a higher percentage of adsorption than Ni/Al and cellulose. With a 49% adsorption capacity in the third cycle, there was a significant decline in adsorption in Ni/Al. This was caused by the exfoliated Ni/Al so it was less stable and ineffective in the absorption of MG in the fourth, fifth, sixth, seventh, and eighth cycles. With an adsorption capacity of 38%, cellulose adsorbent showed a sharp decline in the percentage of adsorbed in the third cycle, causing the adsorption ineffective in cycles four through eight. With a capacity of 54%, the Ni/Al-cellulose demonstrated efficient adsorption up to the sixth cycle. This demonstrates that compared to Ni/Al and cellulose, Ni/Al-cellulose has better structural stability.

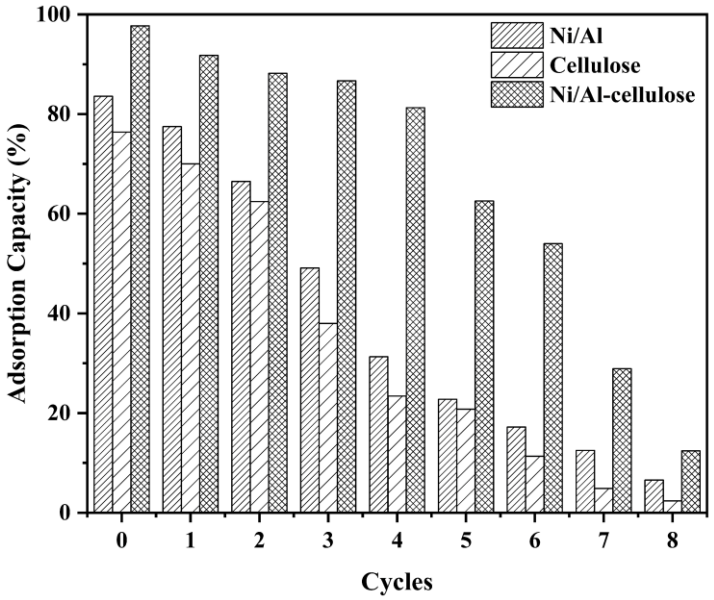

Fig. 12: Reusability of MG on Ni/Al, cellulose, and Ni/Al-cellulose

CONCLUSIONS

The preparation of Ni/Al-cellulose was successful with the co-precipitation method. The MG adsorption capacity for Ni/Al-cellulose showed a result of 107.527 mg/g. A reusability study revealed that Ni/Al-cellulose has a high reusability of up to six cycles with an adsorption capacity of 54%. MG adsorption process in this study follows the Langmuir Isotherm and pseudo second order kinetic model. In this study, the adsorption process occurs through physisorption and chemisorption (physicochemical process) as evidenced by the kinetic data, isotherm data, ΔG value, pH optimum ≠ pH PZC, and FT-IR results which show a shift in wave numbers and changes in peak intensity on the adsorbent after the adsorption process.

Acknowledgements

All authors thank the Research Centre of Inorganic Materials and Coordination Complexes, Sriwijaya University for support of this research.

REFERENCES

[1] Adeyi A. A., Jamil S. N. A. M., Abdullah L. C., Choong T. S. Y. Adsorption of Malachite Green Dye from Liquid Phase Using Hydrophilic Thiourea-Modified Poly(acrylonitrile-co-acrylic acid): Kinetic and Isotherm Studies, *J. Chem.*, **2019**: 1–14 (2019).

[2] Adeyi A. A., Jamil S. N. A. M., Abdullah L. C., Choong, T. S. Y., Lau K. L., N. H. Alias, Simultaneous Adsorption of Malachite Green and Methylene Blue Dyes in a Fixed-Bed Column Using Poly(Acrylonitrile-Co-Acrylic Acid) Modified with Thiourea, *Molecules*, 25(11): 1–17 (2020).

[3] Javaid R., Qazi U. Y. Catalytic Oxidation Process for the Degradation of Synthetic Dyes: An Overview, *Int. J. Environ. Res. Public Health*, **16(11)**: 1–27, (2019).

[4] Lellis B. , Fávaro-Polonio C. Z., Pamphile J. A. and Polonio J. C. Effects of Textile Dyes on Health and the Environment and Bioremediation Potential of Living Organisms, *Biotechnol. Res. Innov.*, **3(2)**: 275–

290 (2019).

[5] Polak J., A. Jarosz-Wilkolazka A. Szuster-Ciesielska M. K., Kamila Wlizlo, Sojka-Ledakowicz J., and J. Lichawska-Olczyk, Toxicity and Dyeing Properties of Dyes Obtained Through Laccase-Mediated Synthesis, *J. Clean. Prod.*, **112**: 4265–4272 (2016).

[6] Shirmardi M., Mahvi A. H., Hashemzadeh B, Naeimabadi A., Hassani G., Niri M. V., The Adsorption of Malachite Green (MG) As a Cationic Dye Onto Functionalized Multi Walled Carbon Nanotubes, *Korean J. Chem. Eng.*, **30(8):** 1603–1608 (2013).

[7] Compound Summary "Malachite Green", https://pubchem.ncbi.nlm.nih.gov/compound/Malachite-green

[8] Suryawan I. W. K., Q. Helmi, S. Notodarmojo, R. Pratiwi, I. Y. Septiariva, Textile Dye Reactive Black 5 (RB5) Bio-Sorption with Moving Bed Biofilm Reactor and Activated Sludge, *Indones. J. Env. Man. Sus.*, **5(2)**: 67-71 (2021).

[9] Ishak Z., S. Salim, D. Kumar, Adsorption of Methylene Blue and Reactive Black 5 by Activated Carbon Derived from Tamarind Seeds, *Trop. Aquat. Soil Pollut.*, **2(1)**: 1–12 (2021).

[10] Ihaddaden, S., Aberkane, D., Boukerroui, A., Robert, D., Removal of Methylene Blue (Basic Dye) by Coagulation-flocculation with Biomaterials (Bentonite and Opuntia ficus indica), *J. Water Process Eng.*, **49**: 102952 (2022).

[11] Sarfo, D. K., Kaur, A., Marshall, D. L., O'Mullane, A. P., Electrochemical Degradation and Mineralisation of Organic Dyes in Aqueous Nitrate Solutions, *Chemosphere*, **316**: 137821 (2023).

[12] Mohamed, W. A. A. El-Gawad, H. H. A., Handal, H. T., et al., Study of Phytotoxicity, Remarkable Photocatalytic Activity, Recycling Process and Energy Consumption Cost of TiO2 Quantum Dots Photocatalyst for Photodegradation of Coomassie Brilliant Blue R Dye, *Opt. Mater. (Amst).*, **137**: 113607 (2023).

[13] Ahmad, N., Suryani Arsyad, F., Royani, I., Mega Syah Bahar Nur Siregar, P., Taher, T., Lesbani, A., High Regeneration of ZnAl/NiAl-Magnetite Humic Acid for Adsorption of Congo Red from Aqueous Solution, *Inorg. Chem. Commun.*, **150**: 110517 (2023).

[14] Sami A. J., Y. N. Butt, S. Nasar, Elimination of a Carcinogenic Anionic Dye Congo Red from Water Using Hydrogels Based on Chitosan, Acrylamide and Graphene Oxide, *J. Bioprocess. Biotech.*, **8(5):**1 (2018).

[15] N'diaye, A. D., Kankou, M. S. A., Hammouti, B., Nandiyanto, A. B. D., Al Husaeni, D. F., A Review of Biomaterial As An Adsorbent: From the Bibliometric Literature Review, The Definition of Dyes and Adsorbent, The Adsorption Phenomena and Isotherm Models, Factors Affecting The Adsorption Process, To The Use of Typha Species Waste As Adsorbent, *Commun. Sci. Technol.*, **7(2)**: 140–153 (2022).

[16] Aoulad El Hadj Ali, Y., Ahrouch, M., Ait Lahcen, A., Demba N'diaye, A., El Yousfi, F., Stitou, M., Dried Sewage Sludge As An Efficient Adsorbent for Pollutants: Cationic Methylene Blue Removal Case Study, *Nanotechnol. Environ. Eng.*, **6(1)**: 1–13 (2021).

[17] Kuntari K. Kinetic and Isotherm Studies of Nitrate Adsorption in Salt Water Using Modified Zeolite, *Bull. Chem. React. Eng. Catal.*, **16(2)**: 286–292 (2021).

[18] Desai, H. K. A., Reddy, G. S. K., Sustainable and Rapid Pillared Clay Synthesis with Applications in Removal of Anionic and Cationic Dyes, *Microporous Mesoporous Mater.*, **352**: 112488 (2023).

[19] Kausar A., Rehman, S. U., Khalid F., et al., Cellulose, Clay and Sodium Alginate Composites for the

Removal of Methylene Blue Dye: Experimental and DFT Studies, *Int. J. Biol. Macromol.*, **209**: 576–585 (2022).

[20] Zubair, M., Aziz, H. A., Ihsanullah, I., Ahmad, M. A., Al-Harthi, M. A., Engineered Biochar Supported Layered Double Hydroxide-cellulose Nanocrystals Composite-: Synthesis, Characterization and Azo Dye Removal Performance, *Chemosphere*, **307**: 136054 (2022).

[21] Abrishamkar, S., Mohammadi, A., De La Vega, J., Wang, D. Y., Kalali, E. N., Layer-by-layer Assembly of Calixarene Modified GO and LDH Nanostructures on Flame Retardancy, Smoke Suppression, and Dye Adsorption Behavior of Flexible Polyurethane Foams, *Polym. Degrad. Stab.*, **207**: 110242 (2022).

[22] Mahmoud R. K., M. Taha, A. Zaher, R. M. Amin, Selective and Highly E?cient Adsorption of a Mixture of Anionic and Cationic Dyes as Synthetic Wastewater Absorbents on Layered Double Hydroxide: Experimental and Computational Studies, *Res. Sq.*, **1**: 1–39 (2021).

[23] Palapa N. R., N. Juleanti, N. Normah, T. Taher, A. Lesbani, Unique Adsorption Properties of Malachite Green on Interlayer Space of Cu-Al and Cu-Al-SiW 12 O 40 Layered Double Hydroxides, *Bull. Chem. React. Eng. Catal.*, **15(3)**: 653–661 (2020).

[24] Brahma D., H. Nath, D. Borah, M. Debnath, H. Saikia, Coconut Husk Ash Fabricated CoAl-Layered Double Hydroxide Composite for the Enhanced Sorption of Malachite Green Dye: Isotherm, kinetics and thermodynamic studies, *Inorg. Chem. Commun.*, **144(8):** 109878 (2022).

[25] Normah, N. R. Palapa, T. Taher, R. Mohadi, H. P. Utami, A. Lesbani, The Ability of Composite Ni/Al-Carbon Based Material Toward Readsorption of iron(II) in Aqueous Solution, *Sci. Technol. Indones.*, **6(3)**: 156–165 (2021).

[26] Ishak W. H. W., I. Ahmad, S. Ramli, M. C. I. M. Amin, Gamma Irradiation-Assisted Synthesis of Cellulose Nanocrystal-Reinforced Gelatin Hydrogels, *Nanomaterials*, **8(10)**: 1–13 (2018).

[27] Allou N. B., A. Yadav, M. Pal, R. L. Goswamee, Biocompatible Nanocomposite of Carboxymethyl Cellulose and Functionalized Carbon–norfloxacin Intercalated Layered Double Hydroxides, *Carbohydr. Polym.*, **186(1)**: 282–289 (2018).

[28] Baunsele A. B. Missa H., Langmuir and Freundlich Equation Test on Methylene Blue Adsorption by Using Coconut Fiber Biosorbent, *Walisongo J. Chem.*, **4(2)**: 131–138 (2021).

[29] Jia N., S.-M. Li, M.-G. Ma, J.-F. Zhu, R.-C. Sun., Synthesis and Characterization of Cellulose-silica Composite Fiber in Ethanol/water Mixed Solvents, *BioResources*, **6(2)**: 1186–1195 (2011).

[30] Zubair M., H. A. Aziz, I. Ihsanullah, M. A. Ahmad, M. A. Al-Harthi, Biochar Supported CuFe Layered Double Hydroxide Composite As A Sustainable Adsorbent for Efficient Removal of Anionic Azo Dye from Water, *Environ. Technol. Innov.*, **23**: 101614 (2021).

[31] Ghosal P. S., A. K. Gupta, Development of a Generalized Adsorption Isothermmodel at Solid-liquid Interface: A Novel Approach, *J. Mol. Liq.*, **240**: 21–24 (2017).

[32] Chung H. K., W.-H. Kim, J. Park, J. Cho, T.-Y. Jeong, P.-K. Park, Application of Langmuir and Freundlich Isotherms to Predict Adsorbate Removal Efficiency or Required Amount of Adsorbent, *J. Ind. Eng. Chem.*, **28**: 241–246 (2015).

[33] Piriya R. S., R. M. Jayabalakrishnan, M. Maheswari, K. Boomiraj, S. Oumabady, Comparative Adsorption Study of Malachite Green Dye on Acid-activated Carbon, *Int. J. Environ. Anal. Chem.*, **103(1)**: 1–15 (2020).

[34] Polak J., Jarosz-Wilkolazka, A., Szuster-Ciesielska, et al., Toxicity and Dyeing Properties of Dyes Obtained through Laccase-mediated Synthesis, *J. Clean. Prod.*, **112**: 4265–4272 (2016).

[35] Adedeji, O, M., Jahan, K., Removal of Pollutants from Aqueous Product of Co-hydrothermal liquefaction: Adsorption and Isotherm Studies, *Chemosphere*, **321**: 138165 (2023).

[36] Yuliasari N., Badri, A. F., Siregar, P. M. S. B. N., Palapa, N. R., Mardiyanto, Mohadi, R., Lesbani, R., Improving the Performance of Mg/Cr LDH by Forming Metal Oxides Mg/Cr-Ni Using Coprecipitation Method as Adsorbent for Cationic Dyes, *J. Ecol. Eng.*, **23(6):** 67–74 (2022).

[37] Iftekhar S., M. E. Küçük, V. Srivastava, E. Repo, M. Sillanpaa, Application of Zinc-aluminium Layered Double Hydroxides for Adsorptive Removal of Phosphate and Sulfate: Equilibrium, Kinetic and Thermodynamic, *Chemosphere*, **209**: 470–479 (2018).

[38] Li, N., Zhidong, C., Dang, H., et al., Deep Eutectic Solvents Assisted Synthesis of MgAl Layered Double Hydroxide with Enhanced Adsorption Toward Anionic Dyes, *Colloids Surfaces A Physicochem. Eng. Asp.*, **591**: 1–10 (2020).

[39] Húmpola, P. D., H. S. Odetti, A. E. Fertitta, J. L. Vicente, Thermodynamic Analysis Of Adsorption Models Of Phenol In Liquid Phase On Different Activated Carbons, *Journal of the Chilean Chemical Society*, **58(1)**: 1541–1544 (2013).

[40] Muinde V. M., J. M. Onyari, B. Wamalwa, J. Wabomba, R. M. Nthumbi, Adsorption of Malachite Green from Aqueous Solutions onto Rice Husks: Kinetic and Equilibrium Studies, *J. Environ. Prot. (Irvine,. Calif).*, **8(3)**: 215–230 (2017).

[41] Gebreslassie Y. T., Equilibrium, Kinetics, and Thermodynamic Studies of Malachite Green Adsorption onto Fig (Ficus cartia) Leaves, *J. Anal. Methods Chem.*, 1–11 (2020).

[42] Nasra E., D. Kurniawati, S. B. Etika, R. Silvia, A. Rahmatika, Effect of pH and Concentration on Biosorption Malachite Green and Rhodamine B Dyes using Banana Peel (Musa balbisiana Colla) as Biosorbent, *J. Phys. Conf. Ser.*, **1788(1):** 1 (2021).

[43] Chaya G., B. A. Khatoon, Malachite Green Dye Removal on Bioadsorbent Nutraceutical Industrialpterocarpus Marsupiumspent, *Int. J. Recent Sci. Res.*, **10**: 30693–30695 (2019).

[44] Lee S., Park, J., Kim, S., Kang, S., Cho, U., Jeon, J., Lee, Y., Seo, D., Sorption Behavior of Malachite Green onto Pristine Lignin to Evaluate the Possibility As A Dye Adsorbent by Lignin, *Appl. Biol. Chem.*, **62(1)**: 1–10 (2019).

[45] Ikhazuangbe P. M., M. . Eruotor, Isothermal and Batch Adsorption Studies of Malachite Green Oxalate Dye onto Activated Carbon from Snail Shell, *Int. J. Environ. Agric. Biotechnol.*, **2(5)**: 2487–2492 (2017).

[46] Dhami D., Homagai P. L., Adsorptive Removal of Malachite Green Dye from Aqueous Solution Using Chemically Modified Charred and Xanthated Wheat Bran, *J. Nepal Chem. Soc.*, **41(1)**: 103–109 (2020).

[47] Sevim F., Lacin O., E. F. Ediza, F. Demir, Adsorption Capacity, Isotherm, Kinetic and Thermodynamic Studies on Adsorption Behaviour of Malachite Green onto Natural Red Clay, *Environ. Prog. Sustain. Energy*, **40(1)**: 1–49 (2021).

[48] Gehlot G., S. Verma, S. Sharma, N. Mehta, Adsorption Isotherm Studies in the Removal of Malachite Green Dye from Aqueous Solution by Using Coal Fly Ash, *Pollut. Res.*, **34(3)**: 647–651 (2015).

[49] Emilia D., Y. M. Hakim, Mohadi R. Mangan Oxide-assisted in Biochar Improvement and Application in MalachiteGreen Removal, *J. Mater. Res.* **1(2)**: 35-43 (2023).

[50] Abhinandan S., S. Dhiraj. Sonochemically Synthesized Mesoporous Pyrophanite-$MnTiO_3/TiO_2$ Nanoparticles: Adsorbent for Removal of Commercial Malachite Green Dye, *Iran. J. Chem. Chem. Eng.*, **41(8)**: 2548-2560 (2022).